Journal of Magnetic Resonance 206 (2010) 183–189

Contents lists available at ScienceDirect

Journal of Magnetic Resonance

journal homepage: www.elsevier.com/locate/jmr

Pneumatic switched angle spinning NMR probe with capacitively coupled double saddle coil

Ilya M. Litvak [a], Catalina A. Espinosa [a], Rebecca A. Shapiro [b], Andrew N. Oldham [a], Vincent V. Duong [a], Rachel W. Martin [a,c,*]

[a] Department of Chemistry, University of California, Irvine, CA 92697-2025, United States
[b] Department of Physics, University of California, Irvine, CA 92697-4575, United States
[c] Department of Molecular Biology and Biochemistry, University of California, Irvine, CA 92697-3900, United States

ARTICLE INFO

Article history:
Received 6 April 2010
Revised 26 June 2010
Available online 29 July 2010

Keywords:
Switched angle spinning
Variable angle spinning
NMR probe
Capacitive coupling
Pneumatic switching

ABSTRACT

Switched angle spinning (SAS) experiments can be used for generating isotropic–anisotropic correlations in oriented samples in a single experiment. In order for these methods to become widespread, specialized hardware is required. Here we describe the electronic and mechanical design and performance of a double-resonance SAS probe. Unlike many previous SAS probe implementations, the focus here is on systems where the dipolar couplings are partially averaged by molecular motion. This probe has a moving double saddle coil capacitively coupled to the stationary circuit. Angle switching is accomplished by a steam engine-type pneumatic mechanism. The speed and stability of the switching hardware for SAS experiments are demonstrated using spectra of model compounds.

1. Introduction

NMR spectroscopy of solids and oriented media is characterized by the trade-off between obtaining isotropic spectra and retaining the structural information contained in the anisotropic interactions. Magic angle spinning (MAS) [1] is the standard method for removing broadening in solids due to magnetic susceptibility differences, chemical shift anisotropy, and dipolar couplings. Heteronuclear and homonuclear dipolar couplings are then selectively reintroduced using one of a large number of recoupling pulse sequences [2]. Much of the success of MAS is due to the development of commercially available spinning hardware. Probes are readily available with extremely stable sample spinning at speeds of 20–30 kHz, and specialized systems can spin at 60 kHz or higher [3]. Switching of the spinning axis as a part of a pulse sequence has found many applications in solids, but is not yet routinely implemented. SAS experiments have most often been used in the context of quadrupolar systems, as the second order quadrupole coupling is a fourth rank spatial tensor that does not average to zero under MAS. Spinning the sample about a time-dependent angle is capable of removing both the first and second order interactions [4–7]. Although the multiple quantum MAS (MQMAS) experiment introduced by Frydman and Harwood [8] made it possible to obtain high-resolution specta for half-integer spin quadrupolar nuclei under MAS, this experiment cannot replace the switched angle or double-rotation techniques completely. For example, it cannot provide high-resolution spectra for nuclei with integer spins [7].

The 2D SAS experiment disentangles the isotropic and anisotropic portions of the spectrum by a 2D Fourier transform in which the direct dimension contains the isotropic spectrum, and spins evolve under anisotropic interactions during the arrayed time t_1. Measuring the chemical shift anisotropy (CSA) was the first application for this type of SAS [9,10]. A modification of the pulse sequence introduced the dipolar couplings [11]. As with MAS, in SAS of solids faster spinning results in better resolution, as demonstrated in an updated SAS experiment using a modified Doty probe capable of spinning up to 20 kHz [12]. SAS experiments have also been used to isolate the spectra of components in mixtures [13]. In a 2D experiment where spin-diffusion occurs at zero angle and the signal is detected at the magic angle, spin-diffusion cross peaks appear only between spins belonging to the same component in a heterogeneous mixture [14]. SAS-type experiments where neither angle is the magic angle have also been used to obtain narrow lines in samples with correlated inhomogeneities [15].

The fast spinning that is an asset in solids, where the dipolar couplings are very strong, is not necessary or desirable in

* Corresponding author at: Department of Molecular Biology and Biochemistry, University of California, Irvine, CA 92697-3900, United States.
E-mail address: rwmartin@uci.edu (R.W. Martin).

1090-7807/$ - see front matter © 2010 Elsevier Inc. All rights reserved.
doi:10.1016/j.jmr.2010.07.001

membranes or other oriented systems. Here, molecular motion partially averages the dipolar couplings, while fast spinning causes instability in the samples. The hardware we describe is optimized for oriented media, with the long-term goal of examining small molecules and proteins in membrane systems. In this case, the spinning is used primarily to align the liquid crystal with the rotor, scaling the dipolar couplings. Liquid crystals in a static sample will align in a strong magnetic field because of their magnetic susceptibility anisotropy $\Delta\chi$. In Variable Angle Spinning (VAS) of liquid crystals, the alignment is dominated by the shear forces produced by spinning; the molecules align parallel or perpendicular to the spinning axis depending on the sign of $\Delta\chi$. This method simplifies the spectra obtained, allowing information about structure and even chirality to be extracted [16–18]. A proof-of-principle SAS COSY experiment on chloropentafluorobenzene in a nematic liquid crystal (I52) [19], showed that splittings due to the dipolar couplings can be correlated with the isotropic chemical shifts in a 2D spectrum. Oriented phospholipid bicelles [20] of the type often used in solution-state NMR structure determination [21] have also been used in SAS [22] and VAS [23,24], giving measurements of dipolar couplings intermediate between those of solids and weakly oriented liquids. The ability to scale the couplings to any degree is especially valuable when dipolar couplings of different magnitude are present in the sample, and when the sample has an inherently strong orientation [25]. While these first experiments illustrate that SAS and VAS on membrane systems and other strongly oriented samples have great potential, there are still technical limitations to be overcome before these methods become widespread.

2. Apparatus

2.1. Contactless resonator with double saddle coil

The central challenge of building an SAS probe is the need for the moving sample coil to be connected to the stationary RF circuit without sacrificing essential aspects of the performance expected from a modern MAS probe. Previously reported strategies include placing the whole spinning assembly inside a stationary coil [26,27], or using a moving coil attached to the rest of the circuit by flexible leads or sliding contacts. These methods are successful to different degrees depending on the application. However, for experiments on oriented membrane samples, the filling factor must be maximized to use the small samples available and the possibility of breakage or instability in the leads must be minimized during long experiments with many points in the indirect dimension. The increased stringency of these requirements is somewhat compensated for by the decreased necessity for high excitation or decoupling fields. While solids applications necessitate maximizing B_1 amplitude for decoupling strong dipolar interactions or exciting the entire bandwidth of a broad quadrupole resonance, samples in oriented media are partially decoupled by molecular motion and field strength is not as important a consideration.

Our probe uses a contactless resonator that is capacitively coupled to the rest of the circuit [28]. The RF coil is connected to the two inner plates of the cylindrical coupling capacitor while the outer plates of the capacitors are fixed and permanently soldered to the tuning network, a tuning tube design [29]. Although traditional MAS probes use a solenoid coil in order to maximize decoupling power, this is not practical for SAS because the direction of the B_1 field precludes effective RF pulses at small angles. Two commonly-used transverse coils are the slotted tube resonator and the saddle coil. An early single-tuned transverse coil was designed to reduce dielectric heating of conductive samples, [30] and modified versions that can be tuned to multiple frequencies are still widely used for this purpose. Although coils of this type have intrinsically less sensitivity than a solenoid of the same size [31], their field direction and homogeneity make them attractive options for applications where a transverse resonator is needed.

The motivation for using a saddle coil in this case is that the slotted tube resonator is a single-loop coil with inherently low inductance. This type of resonator performs best at higher frequencies, so it is well-suited to being used in the ^{1}H-channel of cross-coil designs [32]. One consequence of using it in a double-tuned configuration is low-power delivered on the low frequency channel. The first capacitively coupled probe built in our laboratory using a slotted tube resonator showed good ^{1}H-channel performance and excellent RF homogeneity on both channels, but poor ^{13}C sensitivity, [28], indicating that a higher inductance is necessary for carbon-detected experiments. The required higher inductance can be provided by a saddle coil. The basic version has two pairs of vertical legs connected by semicircular arcs. Double or even triple saddle coils can be made [33], increasing the inductance and improving the field homogeneity. The calculated inductance of a double saddle coil 0.345″ (8.76 mm) long and 0.176″ (4.47 mm) in diameter is approximately 70 nH, as compared to 98 nH for a 7-turn solenoid and 9.2 nH for a slotted tube resonator of the same dimensions. The choice of the coil in this probe is a compromise between the low frequency and high frequency performance. The current probe was designed to deliver a constant RF field strength independent of spinning angle in order to allow for maximum flexibility in testing sample preparations and experiments for SAS in oriented systems. This trade-off may be optimized in future triple-resonance versions by using a cross-coil design with a slotted tube resonator for the proton channel situated orthogonal to either a double-tuned saddle coil or solenoid for the middle and low frequency channels, depending on whether alignment above or below the magic angle is desired.

Fig. 1 shows a diagram of the coil used in our implementation.

2.2. Pneumatic angle switching

Most previous SAS probes have switched the angle using a stepper motor, with switching times ranging from ~1 s in early models [10,9] to less than 30 ms by the 1990s [26,34]. The primary advantage of a stepper motor or servo motor is the flexibility of control. The angle switching can be pre-written into a program for the motor, achieving a high level of complexity for the motion of the spinner. This includes multiple angle settings and even precise control over the acceleration, maximum speed and deceleration of the unit [27]. Ideally, the precision of the angle setting depends only on the minimum step length of the motor. The disadvantage of motor-driven systems is the necessity of locating the magnetic motor far

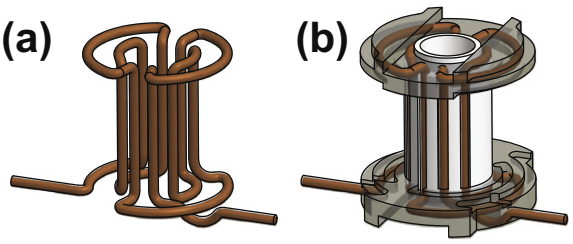

Fig. 1. (a) Double saddle coil made of 22 gauge (0.64 mm diameter) wire. Vertical legs are placed at 0.096″ (2.4 mm) from the spinning axis, at ±45° and ±15° from the desired RF field axis. (b) Because a self-supporting wire gives poor field quality and is prone to misalignment that impairs spinning, the coil radii are supported on the top and on the bottom by machined Kel-F tablets. The vertical coil legs run in the grooves on the outside of the support, as close to the rotor as possible. The inner diameter of the ceramic piece must provide enough room for free rotor spinning. The coil support orifice is 0.136″ with a 0.015″ wall thickness. A 0.030″ deep slot in each support tablet provide room for bearing air exhaust.

enough from the superconducting magnet. The time required to change the spinning axis includes the time to move the mechanical parts plus the time necessary for the spinning rotor to stabilize. To our knowledge, the best switching time so far was achieved with a pneumatic mechanism [14]. Using pneumatics makes it possible to place the switching mechanism close to the spinner module, or even to mount it directly on the spinner. Solenoid valves replace the motor, and are positioned outside the magnet and the mechanical lines and gears are replaced with pressurized air. All the moving parts are located close together in the probe head. The use of air-driven pneumatic cylinders is complicated by factors such as the compressibility of air and slow propagation of pressure waves. However, detailed numerical simulation and modeling of these systems, [35] as well as practical strategies for their implementation [36] have been described.

Here, the angle switching is performed by a steam engine-type pneumatic mechanism, as shown in Figs. 2 and 3. The steam engine mechanism has a geared connection between the piston and the spinner module, making the position of the swinging assembly fully controlled by the position of the piston. An overview of the apparatus is shown in Fig. 2a. The cylinder is mounted between the base plate and the middle plate of the probe body. The vertical position of the cylinder is adjusted through a worm drive. The piston trip is set between the bottom of the cylinder and a separate brake disk, which moves inside the cylinder. It is connected to a threaded rod outside the cylinder through a clip. The brake adjust rod is secured to the base plate and to the middle plate, and also serves as an additional support to the cylinder. To set θ_1 (smaller) and θ_2 (larger), we adjust the vertical position of the pneumatic cylinder and of the brake disk, respectively. The piston is a Rulon disk screwed onto a threaded Delrin rod. Rulon is used because it withstands higher shear stress than Teflon without much increase in friction. The cylinder and the brake disk are machined out of Delrin. The brake disk clip and the adjust rod are brass: due to geometric constraints, a higher tensile strength material is required for these parts.

As in most MAS probes, the rotor spinning speed is measured by an optical tachometer. However, because switching puts strain on the fibers, possibly breaking them or slowing the switching motion, the optical fibers are inserted in the sides of the stator through the drive and bearing air lines as shown in Fig. 2b. Each fiber is separated into a stationary and a moving part, with the ends meeting in the air channels entering the side of the stator. The fiber is passed into the air channel and secured in a holder mounted in the center of the side supports, coaxial with the coupling capacitors. The fiber path is laid out so that the holes in the main body and the top of the stator are in the same plane, and the mouths

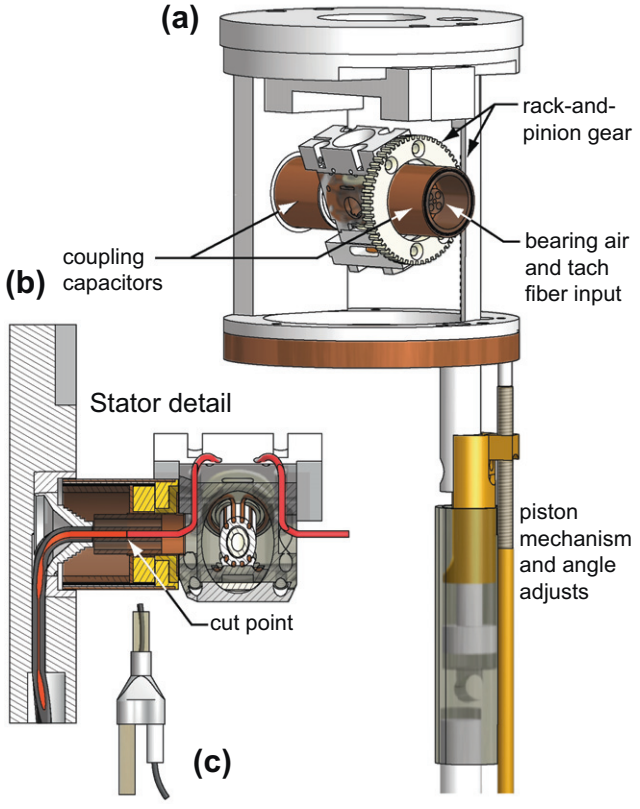

Fig. 2. (a) Overview of the pneumatic SAS probe with the outer can and RF channels removed for clarity, showing the stator and the positioning and actuating mechanisms for the steam engine design. (b) Stator detail showing the fiber optic path. Each fiber has a stationary and a moving part. The moving part of the fiber is stripped of clad and passes through a hole in the side wall of the spinner. Outside, it bends towards the rotor cap, which is 0.085″ in diameter. With the 60° angle between the cables, this means that the fiber holes bypass the center by 0.015″. (c) Y-shaped connectors allow for placing fibers in the drive and bearing air lines without causing air leakage.

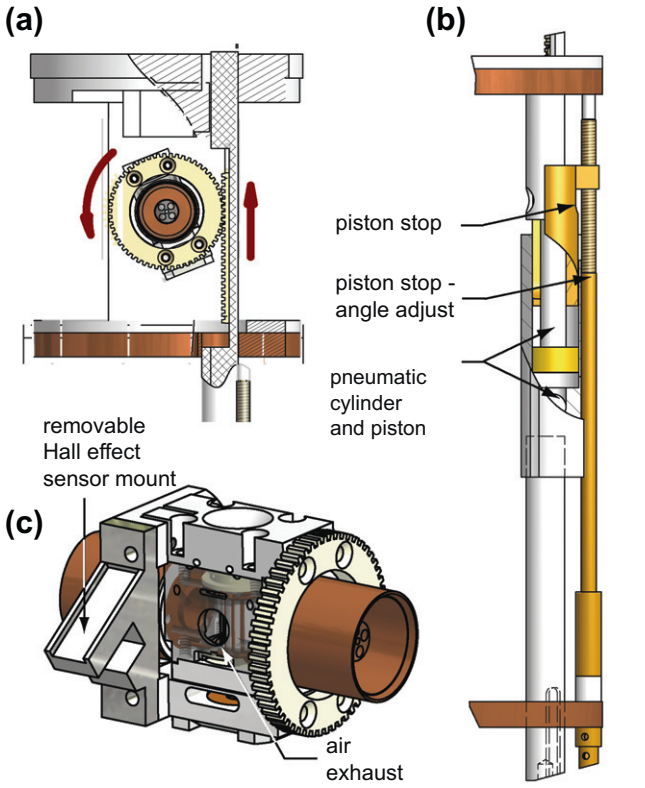

Fig. 3. (a) Linear motion of the piston is converted into the angle switching of the spinner through a rack-and-pinion gear. Molded nylon 14 1/2° pressure angle spur gears and 56-teeth 48-pitch pinion were used. The rack is mounted on a Delrin support rod attached to the piston rod. Its axial alignment is maintained by holes in the base plate and in the top lid of the probe. The top opening is semicircular, preventing rotation of the rack support. (b) The pneumatic cylinder, supported by a 3/8″ Delrin rod, can be moved up or down by an actuator with a 10–24 thread on the bottom. To keep the rod from rotating, it has a 1/8″ slot on the side that accommodates a 4–40 screw in the middle of the copper plate. This combination of the gear pitch diameter and the thread pitch of actuator rods for the cylinder and the brake disk makes the angle adjust 4.1° per knob turn for θ_1, and 3.1° per turn for θ_2. (c) Stator detail showing the coupling capacitors, coil, spinning hardware (Varian 3.2 mm pencil system), and the removable bracket for the Hall effect sensor. In MAS probes, the Hall sensor is usually mounted directly on the stator [37] and calibrated by recording the voltage when the stator is at the magic angle, measured by maximizing the sidebands of KBr [38]. In an SAS probe, the sensor cannot be mounted on the spinner module during an experiment. Thus, the sensor is attached to the stator by a removable bracket and calibrated, with the Hall voltage recorded for a range of angles.

of these holes are then filled to increase the bend radius. The two cuts and the turns reduce the signal transmission efficiency, requiring use of the brightest transmitter and the most sensitive receiver in the line of available Avago HFBR products compatible with our spinner box (Agilent/Varian). A nonmagnetic Vishay Spectrol precision potentiometer is used to adjust the transmitter brightness. Inserting the optical fibers into the air lines enables measurement and control of the spinning frequency at any angle, although fluctuations are observed during a switch from one angle to another.

The SAS pneumatics are actuated by two three-way 12 V DC solenoid valves (ASCO model number 83279041). The pressure valves are synchronized with the Chemagnetics CMX Infinity spectrometer using a TTL pulse written into the pulse program. The output of the TTL channel is 0 volts during the pulse, and +3 V otherwise. Each valve is connected through a TIP-50 transistor, while a D flip-flop alternates the valves. When a valve is being switched off, the EMF produced in the valve solenoid is shorted through a diode. We estimate the time lag due to the finite speed of sound to be 10–20 ms, depending on the length of the tubing. The valves themselves cause another delay: switching a valve requires no less than a 20 ms pulse. These delays can be accounted for in the pulse sequence by sending the TTL pulse earlier. The switching speed also depends on the compressed air pressure, with higher pressure generally giving faster switching. The work cycle of the steam engine mechanism consists of alternating pressure and vacuum applied to the cylinder. The implementation of the pressure line and vacuum pump is diagrammed in Fig. 4. Before the FID collection, an applied pressure pulse rapidly switches the spinning angle to θ_2. The stator is returned back to θ_1 by vacuum applied to the cylinder after the spectrum has been collected. Because vacuum takes more time to build up, this step is slow and is therefore performed during the recycle delay.

3. Results and discussion

3.1. RF performance

In its standard configuration, this probe resonates at two frequencies corresponding to the ^{1}H and ^{13}C frequencies in a 500 MHz (11.74 T) magnet. A tunable trap consisting of an open quarter wave transmission line segment is used to provide a ground path for 500 MHz on the low-frequency side of the coil. The quality factors at the ^{1}H and ^{13}C frequencies are approximately 100 and 250, respectively.

To characterize the RF performance of this probe, we measured the transverse magnetic field B_1 induced in the sample by a unit current. The ratio $\Gamma_f = B_1/\textit{peak input current}$ gives a measure of the probe's ability to produce a B_1 field at a given frequency. The peak input current is $\sqrt{2 \cdot P_{in}/50\Omega}$. This is normalized to factor out the gyromagnetic ratios since $B_1 = \omega_{1k}/\gamma_k$ for nucleus k. For the double saddle coil, $\Gamma = 0.28$ mT/A at 500 MHz and $\Gamma = 1.13$ mT/A at 125 MHz. For comparison, a modified commercial HXY MAS probe with a 7-turn solenoid produced $\Gamma_f = 1.30$ mT/A and 2.16 mT/A at the high and low frequency, respectively. The maximum field strength for the proton channel is 47 kHz with an input power of 380 W, and for the carbon channel it is 76 kHz with an input power of 1000 W. For comparison, a modified commercial probe with a 7-turn solenoid delivered 132 kHz on the proton channel and 87.0 kHz on the carbon channel with the same input powers. Although the maximum ^{1}H decoupling field is quite low compared to a typical MAS probe, it is sufficient for oriented samples where the dipolar couplings are partially motionally averaged. The most common RF failure mode for both channels is arcing of the coupling capacitors. The problem can be minimized by ensuring that the Teflon dielectric fits tightly and protrudes slightly from between the conductive cylinders, leaving no air gap or exposed sharp edges that could induce a corona discharge. If higher fields are applied for prolonged periods of time, breakdown of the Teflon dielectric inside the capacitors can be observed.

One measure of RF homogeneity is a comparison of the signal intensity from a 810° pulse to a 90° pulse from a long nutation array. This value reflects the dephasing of the signal due to field inhomogeneity, as well as the phase inhomogeneity due to the length of the coil. Nutation curves were measured for both channels using a sample of natural abundance adamantane restricted to the homogeneous region of the coil (0.125″ or 3.175 mm). In this probe, the 810° to 90° ratio is 92% at 125 MHz and 73% at 500 MHz. Fig. 5 shows the B_z profile of the double saddle coil. This plot was obtained by connecting the probe to a frequency sweeper and measuring the tuning change due to a small conductive ring placed inside the coil [39]. As expected for a saddle coil, the magnetic field is reasonably homogeneous close to the center of the coil, and rapidly falls off closer to the edges. A region of 0.160″ (about 4 mm) long within the rotor corresponds to a resonance deflection within 90% of the maximum.

The S/N obtained using this probe is lower than but comparable to the MAS probe with the same diameter solenoid coil on both channels. Comparisons were made with a 0.125 mm long adamantane sample, using a one-pulse experiment for ^{1}H, and a direct polarization with ^{1}H decoupling for ^{13}C. For the ^{1}H experiment,

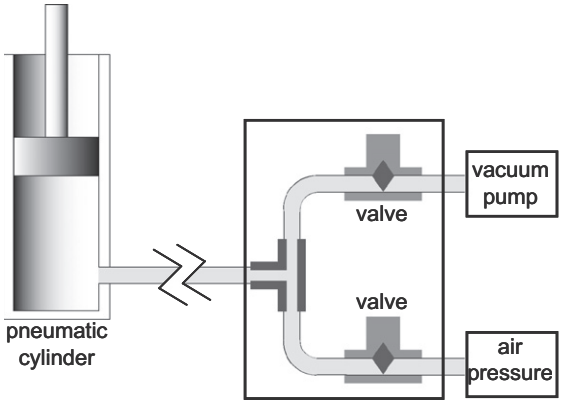

Fig. 4. The SAS motion is controlled by alternating pressure and vacuum. The pneumatic cylinder of the steamer mechanism is connected to a valve box placed outside the magnet via 1/4″ diameter plastic air tubing. Two separate solenoid valves connect the pneumatic system to the vacuum pump and to the external pressure source.

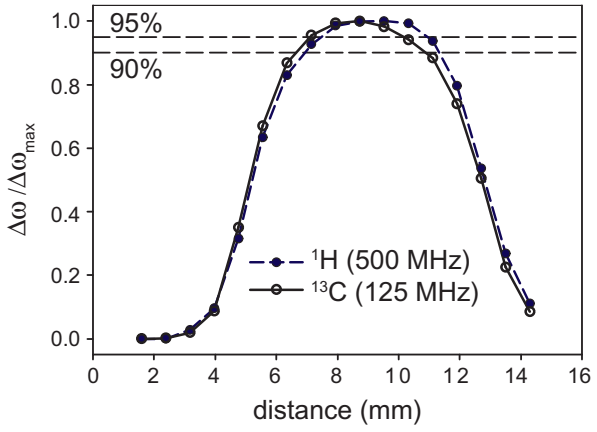

Fig. 5. Field homogeneity of the double saddle coil along the z-axis. The usable sample length is ~4 mm.

the 90° pulse widths were 5.5 μs for the SAS probe and 1.9 μs for the MAS probe, and 4 scans yielded a S/N of 161 for the SAS probe and 169 for the MAS probe. The double saddle coil SAS probe has a broad ^{1}H background from the Macor coil support. The carbon 90° pulse widths were 3.25 μs for the SAS probe and 2.9 μs for the MAS probe and the S/N ratios obtained with 16 scans were 8.2 and 11.6. A cross-polarization match array, demonstrating double-resonance performance is shown in Fig. 6. Experiments to characterize the cross-polarization efficiency at different spinning angles and to optimize low-power cross-polarization performance are underway. The best ^{13}C linewidth achieved so far using this probe was for adamantane with a rotor speed of 18 kHz. The full width at half maximum was approximately 5.6 Hz, while the width of the base is about 35 Hz. Based on variations observed with slightly different coils, coil construction appears to be one factor limiting the linewidth. This linewidth is not ideal, and there is room for improvement in coil construction. However, in practice the spectral resolution of our SAS experiments is usually limited by other factors, such as truncation in the indirect dimension or the difficulties associated with shimming at only one of the two angles used.

3.2. SAS performance

This probe makes use of a 3.2 mm diameter pencil rotor system. Rotors, bearings and drive hardware (tips and brass stator) are purchased from Agilent (Varian), Walnut Creek, CA. The sample volume with standard o-ring plugs is 22 μL. The outer stator (rotor housing) is a homebuilt variation of the commercial design. The important modifications include making the sides flat to accommodate the capacitive coupling rings and drilling holes for the fiber optics and temperature sensor. With this system, stable MAS is achieved up to 18 kHz. Spinning performance is maintained in SAS experiments at rotor speeds up to at least 5 kHz. Since the probe is designed for liquid crystal and membrane systems where fast spinning is not desirable because of sample limitations, it has not been tested with switching at higher rotor speeds. During the approximately nine months that the final version of this probe has been undergoing testing and modifications, only one failure of the switching mechanism was observed. The failure was due to the teeth of the rack-and-pinion gear slipping. Reliable function was restored by strengthening the support rod such that the rack was pressed more firmly against the gear.

The switching speed was measured using a 1-pulse experiment preceded by an angle switch, shown in Fig. 7. The experiment starts with the sample spinning at 0°. A TTL pulse triggers the angle switching mechanism. After a delay time $t_{switch\ delay}$, we apply an ^{1}H 90_x pulse, and collect the 1-dimensional proton spectrum. The linewidth and -shape gives an indication of whether the sample was spinning at the magic angle, off the magic angle, or if the spinning axis was moving during the acquisition time. The angle switch

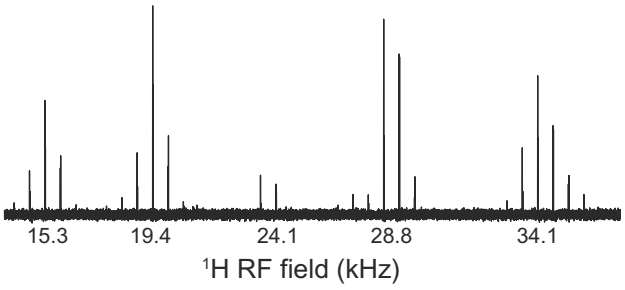

Fig. 6. Cross-polarization match array on adamantane illustrating double-resonance performance. Acquisition parameters: carrier frequency = 125.75 MHz decoupling frequency = 500.09 MHz, spinning speed = 5 kHz, ^{13}C field strength is constant at 24.1 kHz, number of scans = 8, pulse delay = 3 s.

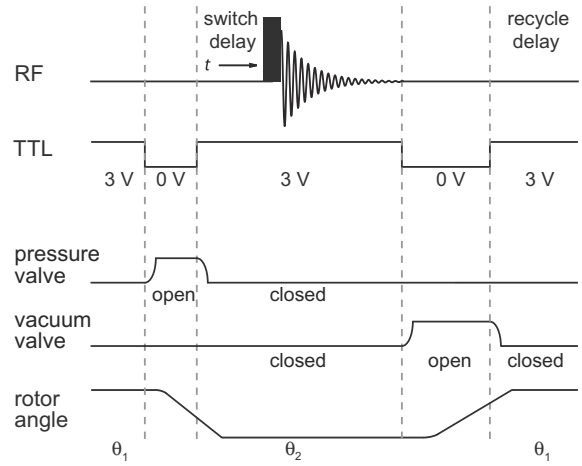

Fig. 7. SAS pulse sequence: a 1-pulse experiment is preceded by an angle switch, with the delay between the switch and the 90° pulse arrayed. The spinner is set to θ_1 before the beginning of the pulse sequence. To switch the angle, the spectrometer sends a TTL pulse. The pulse opens the pressure valve, and the spinner switches to θ_2. The second TTL pulse is sent after the FID collection. This pulse opens the vacuum valve, returning the spinner to the original angle. The second pulse is longer, to give enough time for the vacuum to build up.

time depends on the pressure applied, with higher pressure resulting in faster switching. A side effect is that the vacuum pump needs more time to pump out the air for the reverse trip. To observe the dynamics of the probe, the delay between the TTL pulse and the spectrum collection (switch delay) is arrayed. For a long switch delay the recorded spectrum should look like a standard 1-pulse ^{1}H spectrum. As the delay time becomes shorter, the proton spectrum is collected while the spinning angle is being switched, yielding a broad and distorted line-shape. For even shorter delay times, the spectrum is collected before the sample begins to move from its original off-magic angle position. An example of such an array for 75 psi driving pressure is shown in Fig. 8. The three regimes are clearly distinguishable. The stator does not start to move until after 12 ms after the valve was closed, then it speeds up and reaches the maximum speed by the 20th ms. By the 26th ms the sample is spinning at the magic angle, as revealed by the spinning sidebands. Another time step is necessary for the spinning to stabi-

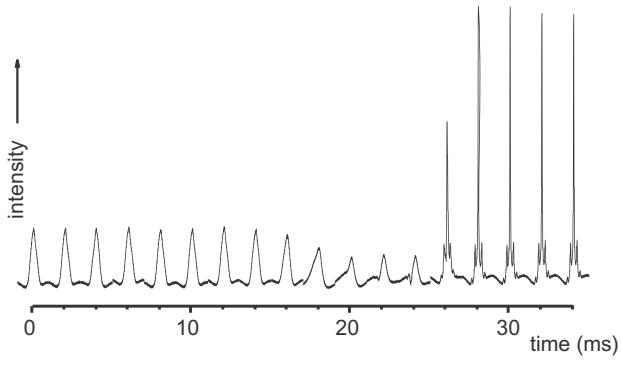

Fig. 8. ^{1}H adamantane spectra acquired with different switching delays, illustrating the motion of the stator. At short delay times, the sample is spinning off the magic angle during acquisition. At intermediate delay times, the stator is moving during acquisition, while longer delay times are needed for it to reach the magic angle and stabilize. The long lag time in the beginning represents the time it takes for the pressurized air to reach the piston, and this delay can be avoided by sending the TTL pulse sooner. Spectra were acquired on a Chemagnetics CMX Infinity spectrometer operating at 500 MHz ^{1}H frequency, with the following acquisition parameters: Carrier frequency = 500.09 MHz, spinning speed = 5.2 kHz, spectral width = 50 kHz, acquisition time = 41 ms, number of scans = 4, pulse delay = 4 s.

lize. The time it takes between when the valve opens and the piston starts moving is due to the finite speed of sound; it takes 12 ms for the pulse of air to travel though the tubing to the piston. This can be compensated for by sending the TTL pulse 12 ms earlier.

Fig. 9 shows the time-domain signal of KBr for different values of the switching delay. With $t = 0$ counted as when the stator begins to move (12 ms from the closing of the valve), it takes 14–16 ms for the stator to reach the magic angle and another ms for the spinning to fully stabilize. The minimum time required for the angle switching with 75 psi input pressure is thus 17 ms, including the time for the spinning to stabilize. Given that the ^{1}H longitudinal relaxation time T_1 is about 0.8–1.2 s for a typical hydrated solid protein sample, this is sufficient for performing the desired experiments. Higher pressure can be used, making the switching faster but at the possible expense of reduced stability. Furthermore, this is the time required for switching from 0° to the magic angle; in order to obtain manageable coupling values, real experiments are likely to require a smaller change in angle. The minimum recycle delay needed to return to 0° from the magic angle is 1 s. Since this is shorter than the recycle delays used for many NMR experiments, the experiment time is not extended by the switching.

The switching speed is also affected by the eddy currents resulting from moving conductors in a magnetic field. Ideally, the coupling capacitor should be designed to maximize capacitance, but in practice the outer diameter (OD) of the conductive rings is limited because increasing their size will also increase the retarding force due to eddy currents. With the gap between plates much less than the diameter, capacitance is nearly proportional to the inner diameter (ID):

$$C = \frac{2\pi\epsilon_0\epsilon \cdot length}{\ln\left(\frac{OD}{ID}\right)} \approx \frac{2\pi\epsilon_0\epsilon \cdot length \cdot ID}{gap}, \quad (1)$$

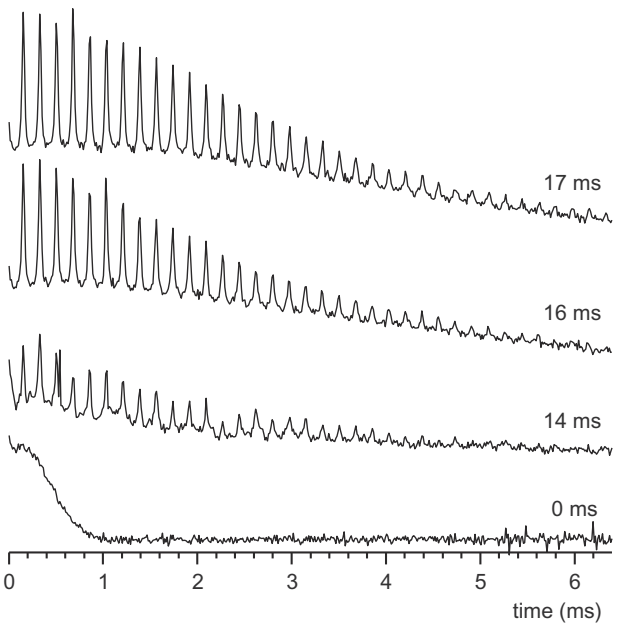

Fig. 9. Time-domain ^{79}Br signals of KBr as a function of switching time. Here $t = 0$ is counted as the time when the stator begins to move, 12 ms after the TTL pulse signaling the closure of the valve. No rotational echoes can be seen at $t = 0$, as the sample is spinning at 0°. 14 ms later, the sample is moving toward the magic angle. At 16 ms, the sample has reached the magic angle, but takes an additional ms to fully stabilize, as can be seen by comparing the small rotational echoes near the end of the acquisition time. 16 scans were taken to confirm reproducibility. Experimental parameters: Carrier frequency = 125.3 MHz, spinning speed = 5.7 kHz, spectral width = 80 kHz, acquisition time = 6.4 ms, pulse delay = 4 s.

When the inner plate of the coupling capacitor moves in the field of the magnet, charge carriers get deflected due to the Lorentz force, and eddy currents slow down the switching. Eddy currents in a rotating conductor have a complex dependence on the shape and speed of the conductor, the conductivity of the material, and its magnetic susceptibility. The simple shape closest to the moving part of our capacitor is the hollow cylinder. According to the analytical solution for the case of an infinitely long hollow cylinder [40], the heat dissipated per unit length of the conductor increases approximately linearly with the outer radius of the cylinder and with the speed of rotation.

The other limiting case for the finite cylinder is a ring (an infinitely short cylinder) with radius r, radial thickness w and axial thickness h. An approximate expression [41] shows cubic dependence of the dissipated heat on h, and linear dependence with respect to the other geometrical parameters. The authors performed a numerical simulation in order to improve the accuracy of the predictions, but their results are not directly applicable to this geometry because they considered a wire loop. The geometry of the cylindrical capacitors is intermediate between these two limiting cases. Even in the absence of a detailed numerical analysis, the eddy currents can be reduced in practical terms by making the pieces as thin as possible, and using Kel-F inserts to provide mechanical rigidity. Copper cylindrical shells with thicknesses of 0.005–0.010″ (0.15–0.20 mm) can be made using conventional machining equipment.

Power dissipation in a conductor due to the eddy currents scales as the square of the external magnetic field [40]. Assuming the same coil dimensions, the capacitance in the contactless RF coupling decreases as $\frac{1}{f_0^2}$, where f_0 is the resonance frequency of the nucleus. The size of the inner plate of the capacitor is reduced accordingly, thus partially alleviating the increase in the dissipated heat. The sizes of other conductive parts of the probe do not change with the field strength. These include the connections between the coil and the moving plate of the capacitor, as well as the drive plate of the spinning system. The contribution from these pieces will grow with the strength of the field, but this contribution is not substantial compared to the coupling capacitor.

4. Conclusion

A ^{1}H–^{13}C double-resonance SAS probe was built using a capacitively coupled double saddle coil. The double saddle coil offers a stable transverse RF field and a good compromise between high-frequency and low frequency performance. The RF characteristics of this coil were characterized, and double-resonance operation was demonstrated.

A pneumatic switching system eliminating the need for a magnetic motor was built and tested for this SAS probe. Factors affecting the switching speed include the dynamics of the pressure and vacuum used to switch the angle, and the eddy currents generated upon moving conductive pieces in a magnetic field. The pneumatic switching was found to be fast and reliable, with switching and stabilization of the rotor complete after 17 ms, as confirmed by measuring the rotational echoes in KBr. As the switching time achieved here is short compared to the typical T_1 of a peptide sample (about 1.5 s), this probe can be used for homonuclear and heteronuclear SAS experiments on small molecules and peptides in oriented systems.

Acknowledgments

This work was supported by the NSF CAREER Grant CHE-0847375. C.A. Espinosa acknowledges support from the Department of Education GAAN fellowship.

The authors acknowledge Lee Moritz and Steve Kaiser for excellent technical assistance.

References

[1] E.R. Andrew, A. Bradbury, R.G. Eades, Nuclear magnetic resonance spectra from a crystal rotated at high speed, Nature 182 (4650) (1958) 1659.

[2] S. Dusold, A. Sebald, Dipolar recoupling under magic-angle spinning conditions, Annual Reports on NMR Spectroscopy, vol. 41, Academic Press Inc., 2000, pp. 185–264.

[3] J.W. Traer, E. Montoneri, A. Samoson, J. Past, T. Tuherm, G. Goward, Unraveling the complex hydrogen bonding of a dual-functionality proton conductor using ultrafast magic angle spinning nmr, J. Magn. Reson. 18 (20) (2006) 4747–4754.

[4] A. Llor, J. Virlet, Towards high-resolution nmr of more nuclei in solids: sample spinning with time-dependent spinner axis angle, Chem. Phys. Lett. 152 (2, 3) (1988) 248–253.

[5] K. Mueller, B. Sun, G. Chingas, J.Q. Zwanziger, T. Terao, A. Pines, Das of quadrupolar nuclei, J. Magn. Reson. 86 (1990) 470.

[6] P. Grandinetti, The Encyclopedia of NMR, Wiley, 1996 (Chapter: Dynamic Angle Spinning, pp. 1768–1776).

[7] A. Jerschow, From nuclear structure to the quadrupolar nmr interaction and high-resolution spectroscopy, Prog. Nucl. Magn. Reson. Spectrosc. 46 (1) (2005) 63–78.

[8] L. Frydman, J. Harwood, isotropic spectra of half-integer quadrupolar spins from bidimensional Magic Angle Spinning NMR, J. Am. Chem. Soc. 117 (19) (1995) 5367–5368.

[9] A. Bax, N. Szeverenyi, G. Maciel, Chemical shift anisotropy in powdered solids studied by 2d ft nmr with flipping of the spinning axis, J. Magn. Reson. 55 (1983) 494–497.

[10] T. Terao, T. Fujii, T. Onoderra, A. Saika, Switching-angle sample spinning nmr spectroscopy for obtaining powder-pattern-resolved 2d spectra: measurements of 13c chemical shift anisotropies in powdered 3,4-dimethoxybenzaldehyde, Chem. Phys. Lett. 107 (2) (1984) 145–148.

[11] T. Terao, H. Miura, A. Saika, Dipolar sass nmr spectroscopy: separation of heteronuclear dipolar powder patterns in rotating solids, J. Chem. Phys. 85 (7) (1986) 3816–3826.

[12] T. Mizuno, K. Takegoshi, T. Terao, Switching-angle spinning nmr probe with a commercially available 20 kHz spinning system, J. Magn. Reson. 171 (2004) 15–19.

[13] R. Tycko, Normal angle spinning dipolar spectroscopy for structural studies by solid-state nuclear magnetic resonance, J. Am. Chem. Soc. 116 (5) (1994) 2217–2218.

[14] M. Tomaselli, B.H. Meier, M. Baldus, J. Eisenegger, R. Ernst, An rf-driven nuclear spin-diffusion experiment using zero-angle sample spinning, Chem. Phys. Lett. 225 (1994) 131–139.

[15] D. Sakellariou, C.A. Meriles, R.W. Martin, A. Pines, High-resolution nmr of anisotropic samples with spinning away from the magic angle, Chem. Phys. Lett. 377 (2003) 333–339.

[16] J. Courtieu, J.P. Bayle, B.M. Fung, Variable angle sample spinning nmr in liquid crystals, Prog. Nucl. Magn. Reson. Spectrosc. 26 (Part 2) (1994) 141–169.

[17] T. Väänänen, J. Jokisaari, M. Seläntaus, A variable angle spinning system for the determination of NMR parameters of liquid-crystalline samples, J. Mag. Reson. 72 (3) (1987) 414–421.

[18] L. Beguin, J. Courtieu, L. Ziani, D. Merlet, Simplification of the h-1 nmr spectra of enantiomers dissolved in chiral liquid crystals, combining variable angle sample spinning and selective refocusing experiments, Magn. Reson. Chem. 44 (12) (2006) 1096–1101.

[19] R. Havlin, G. Park, T. Mazur, A. Pines, Using switched angle spinning to simplify nmr spectra of strongly oriented samples, J. Am. Chem. Soc. 125 (26) (2003) 7998–8006.

[20] C.R. Sanders, B.J. Hare, K.P. Howard, J.H. Prestegard, Magnetically-oriented phospholipid micelles as a tool for the study of membrane-associated molecules, Prog. Nucl. Magn. Reson. Spectrosc. 26 (1994) 421–444.

[21] A. Bax, A. Grishaev, Weak alignment nmr: a hawk-eyed view of biomolecular structure, Curr. Opin. Struct. Biol. 15 (5) (2005) 563–570.

[22] G. Zandomeneghi, M. Tomaselli, J.D. van Beek, B.H. Meier, Manipulation of the director in bicellar mesophases by sample spinning: A new tool for nmr spectroscopy, J. Am. Chem. Soc. 123 (5) (2001) 910–913.

[23] N. Lancelot, K. Elbayed, A. Bianco, M. Piotto, Measurement of scaled residual dipolar couplings in proteins using variable-angle sample spinning, J. Biomol. NMR 29 (3) (2004) 259–269.

[24] N. Lancelot, K. Elbayed, M. Piotto, Applications of variable-angle sample spinning experiments to the measurement of scaled residual dipolar couplings and n-15 csa in soluble proteins, J. Biomol. NMR 33 (3) (2005) 153–161.

[25] A.I. Kishore, J.H. Prestegard, Molecular orientation and conformation of phosphatidylinositides in membrane mimetics using variable angle sample spinning (vass) nmr, Biophys. J. 85 (6) (2003) 3848–3857.

[26] K.T. Mueller, G.C. Chingas, A. Pines, Nmr probe for dynamic-angle spinning, Rev. Sci. Instrum. 62 (6) (1991) 1445–1452.

[27] F.D. Doty, The Encyclopedia of NMR, vol. 7, Wiley, 1996 (Chapter: Solid State NMR Probe Design, pp. 4475–4485).

[28] C. Qian, A. Pines, R.W. Martin, Design and construction of a contactless mobile rf coil for double resonance variable angle spinning nmr, J. Magn. Reson. 188 (1) (2007) 183–189.

[29] R.W. Martin, E. Paulson, K.W. Zilm, Design of a triple resonance magic angle sample spinning probe for high field solid state nuclear magnetic resonance, Rev. Sci. Instrum. 74 (6) (2003) 3045–3061.

[30] D. Alderman, D. Grant, Efficient decoupler coil design which reduces heating in conductive samples in superconducting spectrometers, J. Magn. Reson. 36 (3) (1979) 447–451.

[31] D. Hoult, R. Richards, The signal-to-noise ratio of the nuclear magnetic resonance experiment, J. Magn. Reson. 24 (1976) 71–85.

[32] C.V. Grant, Y. Yang, M. Glibowicka, C.H. Wu, S.H. Park, C. Deber, S. Opella, A modified alderman-grant coil makes possible an efficient cross-coil probe for high field solid-state nmr of lossy biological samples, J. Magn. Reson. 201 (2009) 87–92.

[33] T.G. Ajithkumar, E.R.H. van Eck, A.P.M. Kentgens, Homonuclear correlation experiments for quadrupolar nuclei, spinning away from the magic angle, Solid State Nucl. Magn. Reson. 26 (3–4) (2004) 180–186.

[34] M.A. Eastman, P.J. Grandinetti, Y.K. Lee, A. Pines, Double-tuned hopping-coil probe for dynamic-angle-spinning nmr, J. Magn. Reson. 98 (2) (1992) 333–341.

[35] E. Richer, Y. Hurmuzlu, A high performance pneumatic force actuator system: Part i – nonlinear mathematical model, J. Dyn. Syst. Meas. Control 122 (2000) 416–425.

[36] E. Richer, Y. Hurmuzlu, A high performance pneumatic force actuator system: Part ii – nonlinear controller design, J. Dyn. Syst. Meas. Control 122 (2000) 426–434.

[37] S. Mamone, A. Dorsch, O.G. Johannessen, M.V. Naik, P.K.L.M.H. Madhu, A hall effect angle detector for solid-state nmr, J. Magn. Reson. 190 (1) (2008) 135–141.

[38] J.S. Frye, G.S. Maciel, Setting the magic angle using a quadrupolar nuclide, J. Magn. Reson. 48 (1982) 125–131.

[39] E. Paulson, R.W. Martin, K.W. Zilm, Cross polarization, radio frequency field homogeneity, and circuit balancing in high field solid state nmr probes, J. Magn. Reson. 171 (2004) 314–323.

[40] M. Perry, Low frequency electromagnetic design, Electrical Engineering and Electronics, vol. 28, Marcel Dekker, 1985.

[41] P. Aguiar, J.-F. Jacquinot, D. Sakellariou, Experimental and numerical examination of eddy (foucault) currents in rotating micro-coils: generation of heat and its impact on sample temperature, J. Magn. Reson. 200 (2009) 6–14.